ACS OMEGA

http://pubs.acs.org/journal/acsodf

Article

Evolution of "On-Barcode" Luminescence Oxygen Channeling Immunoassay by Exploring the Barcode Structure and the Assay System

Zuying Feng, Qingsheng Guo,* Yao Wang, Yunfei Ge, Zhiying Zhang, Yan Wu, Qilong Li, Hajar Masoomi, Hongchen Gu, and Hong Xu*

Cite This: *ACS Omega* 2022, 7, 2344−2355

Read Online

ACCESS | Metrics & More | Article Recommendations | Supporting Information

ABSTRACT: The multiplexed luminescence oxygen channeling immunoassay (multi-LOCI) platform we developed recently that combines conventional LOCI and suspension array technology is capable of realizing facile "mix-and-measure" multiplexed assays without tedious washing steps. However, previous work lacks comprehensive studies of the structure−performance relationship of the host−guest-structured barcode, which may obstruct the evolution and further translation of this exciting new technology to practical applications. Accordingly, this work revealed that polyelectrolyte interlayers played a crucial role in tuning the packing density of guest acceptor beads (ABs). More interestingly, we noticed that "sparse" barcodes (barcodes with low ABs packing density) exhibited comparable assay performance with "compact" ones (barcodes with high ABs packing density). The high robustness of barcodes allows for multi-LOCI to be a more universal and flexible assay platform. Furthermore, through optimization of the assay system including the laser power, as well as the concentrations of donor beads and biotinylated detection antibodies, the multi-LOCI platform showed a significant improvement in sensitivity compared with our previous work, with the limit of detection decreasing to as low as ca. 1 pg/mL. Impressively, multi-LOCI that enabled simultaneous detection of multiple analytes exhibited comparable sensitivity with the classical single-plexed LOCI, due to the ingenious structural design of the multi-LOCI barcode and the unique "on-barcode" assay format.

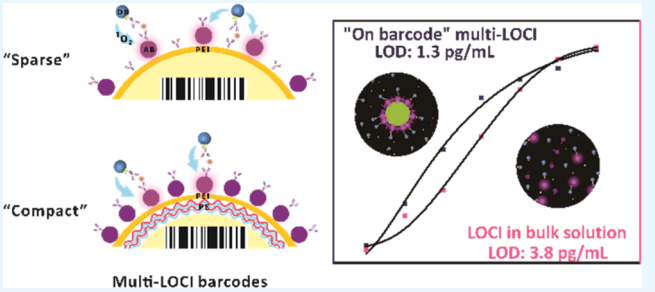

1. INTRODUCTION

Multiplexed assays are of great interest to life sciences and biomedical fields including gene analysis,[1,2] drug delivery and screening,[3] and disease diagnostics[4−8] due to their capacity of detecting multiple targets simultaneously within one reaction. Compared with traditional planar-array-based biochips that are widely used in the discovery of biomarkers and semi-quantitative detection, encoded bead-based suspension arrays, which are capable of addressing and capturing corresponding multiple target molecules, high reaction efficiency, high flexibility in target selection, and tremendous coding capability,[9,10] are a promising technology for multiplex quantitative assays. After Luminex Corporation successfully launched xMAP technology,[11−13] more efforts have continuously been made toward developing new coding strategies for the sake of expanding the barcode libraries.[9,14−17]

In addition to proposing new encoding strategies, remarkably fast-growing progress has also been made in developing novel detection methodologies based on barcodes, aiming at higher performance or ease of operation.[18−21] Recently, through the combination of encoded beads with luminescence oxygen channeling immunoassay (LOCI) technology, our group developed a novel suspension array platform, called "multi-LOCI".[22] As shown in Scheme 1a, a dual-functional multi-LOCI barcode consists of two isolated building blocks: (a) encoded host beads (EHBs) that offer barcode signals for the identification of multiple analytes and (b) LOCI acceptor beads (ABs), which are immobilized onto the surface of EHBs (EHB@ABs) and provide LOCI signals to quantify specific analyte concentrations. For a typical multi-LOCI assay, the analytes of interest are specifically captured by EHB@ABs, further leading to the specific bounding of biotinylated detection antibodies and streptavidin-coated donor beads (DB-SA) via formation of immune complexes. Upon excitation of DB-SA at 680 nm, singlet oxygen molecules transfer from DB-SA to ABs and trigger strong chemiluminescence emission at 615 nm,[23,24] and both barcode and LOCI signals are acquired via image analysis processing. This strategy achieves a

Received: November 5, 2021
Accepted: December 23, 2021
Published: January 5, 2022

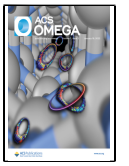

https://doi.org/10.1021/acsomega.1c06236
ACS Omega 2022, 7, 2344−2355

Scheme 1. Schematic Illustration of (a) the Principle of Multi-LOCI for Multiplexed Assay and Key Issues That Were Investigated in This Research Including the (b) Multi-LOCI Barcode Structure and (c) Assay System as Indicated

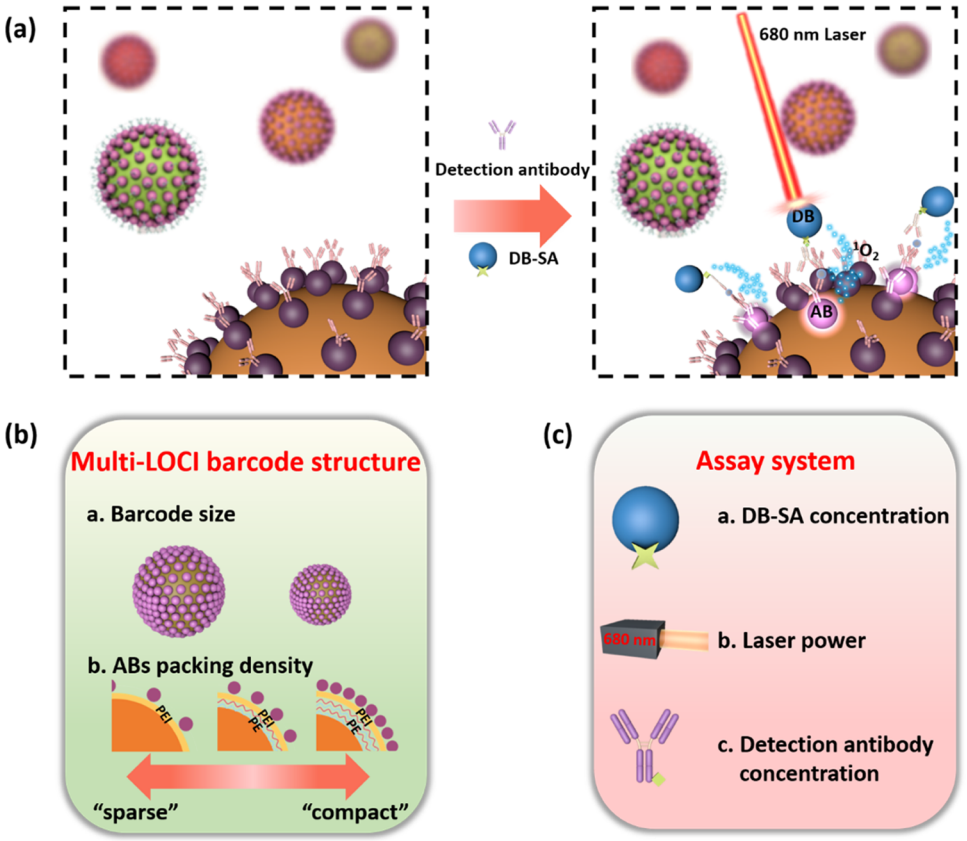

unique multiplexed assay following a simple "mix-and-measure" protocol without the need for tedious washing steps, which is very promising for the development of multiplexed point-of-care test technology.

The multi-LOCI technique exhibits the capacity of both high multiplexing and ease of operation. However, the lack of comprehensive studies of the structure−performance relationship of the unique host−guest barcodes hinders the evolution of this promising technology to a universal and practical method. First, this study systematically investigated the structure−performance relationship of multi-LOCI barcodes from two aspects that are shown in Scheme 1b. On the one hand, the barcode size was explored because it might be closely related to the encoding capacity, reaction kinetics, and the accuracy of imaging-based decoding. On the other hand, by adjusting the number of polyelectrolyte interlayers, the packing density of ABs was found to be precisely controlled, providing a guideline to establish a robust and flexible multi-LOCI barcode fabrication protocol. More importantly, this discovery would pave a novel but universal pathway for construction of host−guest-structured micro- and nanocomposites. A deeper investigation on the relationship between packing density and assay performance was explored since the number of ABs loaded on a single barcode was supposed to directly influence the LOCI signal. Second, there is still much room for detection performance improvement of the multi-LOCI assay system, which is not investigated in detail in our previous study. As shown in Scheme 1c, the multi-LOCI assay system including DB-SA concentration, the 680 nm laser power, and the concentrations of biotinylated detection antibodies for specific analytes was comprehensively optimized to clarify the potential relationship between these parameters and the detection performance, which in turn enabled improved sensitivity. Through the elaborate investigations of both the barcode structure and the assay system, the multi-LOCI was supposed to be demonstrated as a more powerful platform with high robustness and excellent performance.

2. EXPERIMENTAL SECTION

2.1. Materials. Multi-LOCI EHBs with a diameter of 3 and 6 μm were prepared following the procedure described in our previous studies.[14,25] By adjusting the fluorescence intensities of fluorescein isothiocyanate (FITC) and rhodamine isothiocyanate (RITC), 3 μm EHBs with 28 different barcodes (combinations of seven levels of FITC and four levels of RITC) and 6 μm EHBs with 30 different barcodes (combinations of six levels of FITC and five levels of RITC) were obtained, respectively. Poly(sodium 4-styrenesulfonate) (PSS, M_w = 70k), poly(diallydimethylammonium chloride) (PDDA, 100k ≤ M_w ≤ 200k), *N*-(3-dimethylaminopropyl)-*N*′-ethylcarbodiimide hydrochloride (EDC), *N*-hydroxysuccinimide (NHS), 2-(*N*-morpholino)ethanesulfonic acid monohydrate (MES), 4-(dimethylamino)pyridine (DMAP), 2-iminothiolane hydrochloride (ITL), 5,5′-dithiobis(2-nitrobenzoic acid) (DTNB), DL-dithiothreitol (DTT), and poly(ethylenimine) (PEI, M_w = 10k) were purchased from Sigma-Aldrich. Traut's Reagent was prepared by dissolving ITL (40 mM) and DMAP (40 mM) in ethanol. Ellman's Reagent was a PBS (10 mM, pH 7.4) buffer containing 3.53 mM DTNB and 1 mM EDTA. Cysteine was bought from

https://doi.org/10.1021/acsomega.1c06236
ACS Omega 2022, 7, 2344−2355

Macklin. Carboxyl-modified ABs and DB-SA were obtained from PerkinElmer. Anti-IFN-γ capture antibody, anti-IL-10 capture antibody, and biotinylated anti-IL-10 detection antibody were obtained from Biolegend. Anti-IFN-γ detection antibody, IL-6, IL-17A, IL-10, and the corresponding antibodies of IL-6 and IL-17A were provided by R&D Systems. IFN-γ was provided by Hytest.

2.2. Preparation of Multi-LOCI Barcodes. *2.2.1. Deposition of Polyelectrolyte Multilayers on Encoded Host Beads.* Through the electrostatic interaction between the positively charged PDDA and negatively charged PSS,[26] multilayered polyelectrolytes were deposited on silica-encapsulated EHBs (EHB@SiO_2), and the preparation process was as follows. EHB@SiO_2 was dispersed in PDDA solution (5 mg/mL, in 0.5 M NaCl), rotated for 20 min, and then washed with deionized water. The obtained beads were then dispersed in PSS solution (5 mg/mL, in 0.5 M NaCl) with rotation for 20 min and were further washed with deionized water. By repeating this procedure several times, PDDA and PSS were alternately encapsulated onto the surface of EHBs. The obtained beads were denoted as EHB@(PSS/PDDA)*n*, where *n* (from 0 to 4) indicates the number of PSS/PDDA pairs. Finally, EHB@(PSS/PDDA)*n*@PEI was obtained by suspending beads in PEI solution (50 mg/mL, in 10 mM MEST) with rotation for another 20 min, followed by washing six times.

2.2.2. Quantification of Surface Primary Amino Groups of EHB@(PSS/PDDA)n@PEI. The ITL/DTNB method was used to quantify the surface primary amino groups.[27−29] ITL and DTNB are known as Traut's Reagent and Ellman's reagent, respectively. Typically, 0.5 mg of EHB@(PSS/PDDA)*n*@PEI (*n* from 0 to 4) were washed with ethanol twice and dispersed in 400 μL of Traut's Reagent. After the mixture reacted for 1 h, beads were washed with ethanol, 1 mmol/L DTT, ethanol, and PBS sequentially. Then, the beads were suspended in 203.5 μL of PBS and reacted with 10 μL of Ellman's reagent for 15 min. By comparing the sample's absorbance at 412 nm measured by a SpectraMax i3 multimode microplate reader (Molecular Devices, CA) with a standard curve of cysteine, the content of sulfhydryl groups was calculated, and then the density of the amino group on the surface of EHB@(PSS/PDDA)*n*@PEI was obtained.

2.2.3. Fabrication of Host−Guest-Structured Multi-LOCI Barcodes. Through a carbodiimide reaction, carboxylated ABs were immobilized covalently on amino-functionalized EHB@(PSS/PDDA)*n*@PEI host beads to achieve multi-LOCI barcodes. The detailed assembly process of this host−guest-structured multi-LOCI barcodes was as follows. First, 1.3 mg of EHB@(PSS/PDDA)*n*@PEI dispersed in 150 μL of 100 mM MES was dropwise added into a suspension containing 0.6 mg of ABs, followed by rotation for 30 min. Then, 100 μL of 100 mg/mL EDC and NHS were, respectively, added into the mixture followed by rotation for 3 h at room temperature. Afterward, 2.5 mM sodium hydroxide (NaOH) and water were used to sequentially wash the as-synthesized host−guest-structured EHB@(PSS/PDDA)*n*@PEI@ABs (denoted as EHB@ABs). To remove the residual amino group of the multi-LOCI barcodes, 150 μL of PAA solution (1 mg/mL, in 10 mM MEST, pH 5.0) was added to the as-synthesized EHB@ABs with rotation for 30 min at room temperature. Then, 150 μL of EDC solution (10 mg/mL, in 10 mM MEST, pH 5.0) was added into the mixture and reacted for 2 h, and the beads were washed and stored in water finally.

2.3. Bioconjugation and Immunoassay. *2.3.1. Bioconjugation of EHB@ABs with Capture Antibody.* Capture antibodies were conjugated to EHB@ABs via the carbodiimide reaction, and the protocol was as follows. First, 2.6 mg of EHB@ABs was washed and dispersed in 400 μL of MEST buffer (10 mM, pH 5.0) containing 10 mg of EDC and 10 mg of NHS. The mixture was reacted for 20 min and then was washed with MEST buffer twice. After the activation of carboxyl groups on the beads, 0.1 mg of capture antibodies were added and incubated for 2 h at 37 °C. The beads were washed using PBS twice after the reaction. To block the unreacted active NHS, beads were suspended in 400 μL of PBS containing 0.5 wt % bovine serum albumin (BSA) and 0.3 wt % glycine, followed by overnight incubation at 4 °C. After the blocking process, the conjugated beads were washed and stored in a PBS solution containing 0.1 wt % BSA. The amount of immobilized capture antibodies of EHB@ABs was quantified by the BCA protein quantification kit through the depletion method. The amounts of conjugated capture antibodies for IFN-γ, IL-17A, IL-10, and IL-6 were calculated to be 1.51, 1.12, 1.43, and 1.43 pg/bead, respectively.

2.3.2. Multi-LOCI Assay. In general, the immunoassay procedure of multi-LOCI was as follows. Four kinds of multi-LOCI EHB@ABs (4000 for each type EHB@ABs) conjugated with four specific capture antibodies (IFN-γ, IL-6, IL-10, IL-17A) and the corresponding biotinylated detection antibodies were added into 100 μL of PBS buffer containing a series concentration of analytes. After incubation for 1 h at 37 °C, DB-SA were added and incubated for another 1 h at 37 °C. A fluorescence microscope was used to acquire barcode information and the mean LOCI intensity of the corresponding barcode, and then the obtained data was analyzed through customized MATLAB (MathWorks) software. In addition, for the optimized experiment of establishing the multiplexed calibration curves, the incubation time of both steps was 30 min.

2.3.3. Conventional LOCI Assay. First, 15 μL of ABs conjugated with anti-IFN-γ capture antibody (33 μg/mL), IFN-γ, and biotinylated anti-IFN-γ detection antibody (2 μg/mL) was mixed and incubated for 1 h at 37 °C. Then, 35 μL of DB-SA (60 μg/mL) was added. After being incubated for another 1 h at 37 °C, 35 μL of the sample was pipetted into a 384-well plate, followed by a signal readout on the microplate reader.

2.3.4. Characterizations. The morphology and size of EHBs and EHB@ABs were characterized using a Zeiss Ultra Plus field emission scanning electron microscope (SEM, Carl Zeiss AG, Germany) operated at an accelerating voltage of 5 kV. ζ-Potential was recorded using a Zetasizer Nano ZSP (Malvern, U.K.). The number of beads was calculated via flow cytometry analysis on a NovoCyte 2040R instrument (ACEA). Acquisition of multi-LOCI signal was carried out via a fluorescence microscope (IX83, Olympus) equipped with a 680 nm laser diode (Changchun New Industries, Changchun, China) and an LED light (Lumencor) using a 10× objective. In short, the LOCI signal was excited by a 680 nm laser and collected by an sCMOS camera (Prime BSI, Photometrics) at 615/20 nm. The barcode signals and FITC and RITC fluorescence were excited by the LED light at 466/40 and 554/23 nm with emission collected at 525/50 and 609/54 nm by the camera, respectively. To evaluate the uniformity and amount of assembled ABs, the fluorescence of ABs loaded on EHBs was directly excited by the LED light at 378/52 nm with

https://doi.org/10.1021/acsomega.1c06236
ACS Omega 2022, 7, 2344−2355

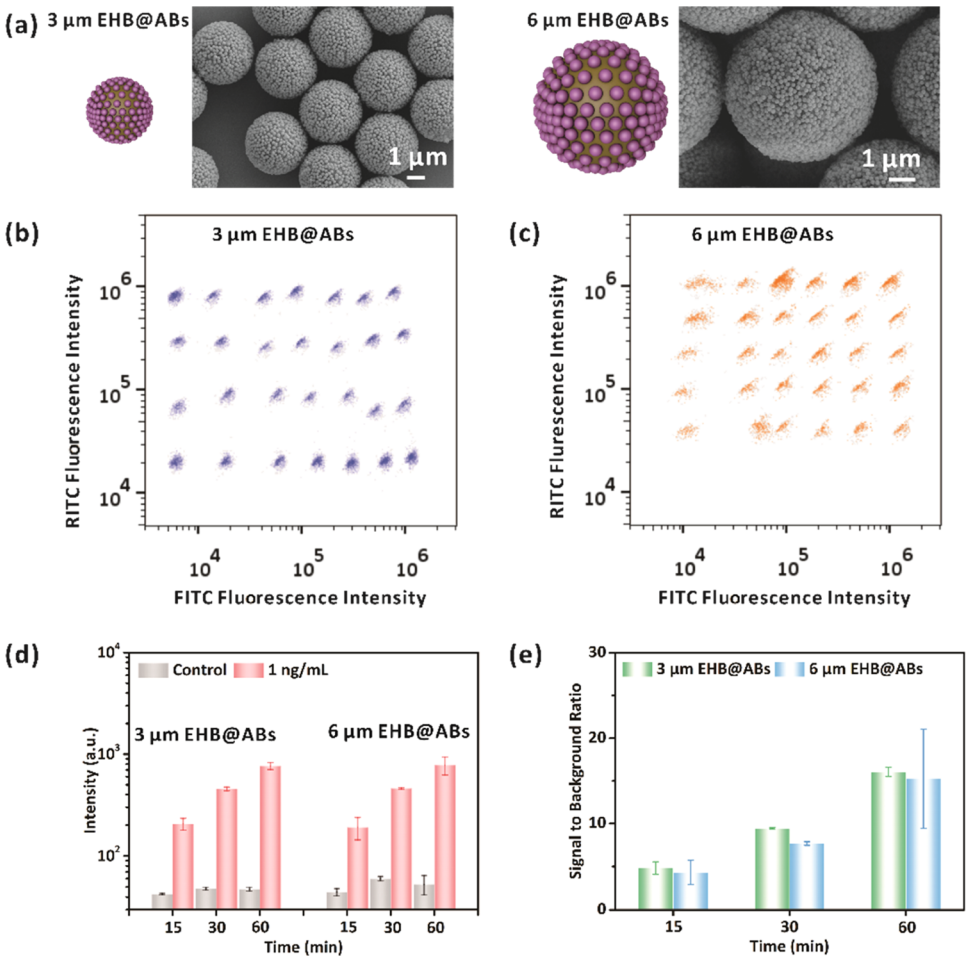

Figure 1. (a) Scheme and SEM images of 3 and 6 μm multi-LOCI barcodes. (b, c) Scatter plots of the library of the 3 and 6 μm barcodes obtained by imaging-based decoding, respectively. (d) Mean LOCI intensities of 3 and 6 μm multi-LOCI barcodes detecting 1 and 0 ng/mL IFN-γ at different time points. (e) Bar plot of the corresponding signal-to-background ratios in (d).

emission collected at 615/20 nm. Two images including barcode signals from FITC and RITC channels were, respectively, acquired, followed by image acquisition of LOCI signal. Then, image analysis was realized by the customized MATLAB software. First, all images were pretreated to reduce the background noises. Then, the fluorescent intensities of all beads in FITC and RITC channels were recognized by an appropriate threshold and then screened by setting proper parameters of the recognized regions including diameter, area, and circularity of the barcodes in images. Afterward, gray values of the recognized beads in the FITC, RITC, and LOCI channels were, respectively, extracted. The extracted gray values in the FITC and RITC channels were used to identify which code they were, and the gray values in the LOCI channel were used to determine the concentration level of the corresponding analytes.

3. RESULTS AND DISCUSSION

3.1. Effect of Barcode Size on the Detection Performance of the Multi-LOCI System. As the core element of multi-LOCI, EHB@ABs, the host−guest-structured multi-LOCI barcode acts as a dual-functional microcarrier that enables high multiplexed capability and a facile detection strategy. Thus, it is essential to investigate the structural property of EHB@ABs, as well as its effect on the performance of the platform. As mentioned in the scheme before, the size of EHBs should be properly controlled in an appropriate range considering the coding capacity, reaction kinetics, and accuracy of imaging decoding. Large EHBs possess lower reaction efficiency; thus, they require vigorous mixing to ensure themselves in a uniform suspension state, which may damage target molecules and even the EHBs.[30] However, if the EHBs are too small, the following problems cannot be ignored: (a) encoding capacity is limited as smaller beads provide less space for embedding fluorescent dyes,[25] (b) a higher-magnification objective lens is needed to guarantee decoding accuracy, which increases the cost and complexity of the equipment, and (c) the number of ABs loaded on a single barcode is limited due to the smaller surface area, which may influence the detection LOCI signal. Therefore, considering both the previous reports on barcodes[31] and the specific requirements of multi-LOCI barcodes described above, the appropriate size for multi-LOCI EHBs is in the range of 3−10 μm. As a demonstration, barcodes with diameters of 3 and 6 μm were employed to explore how the barcode size influenced the detection performance. As shown in SEM images (Figure 1a), both 3 and 6 μm multi-LOCI EHBs are well-assembled with high-density ABs. It is worth noting that both 3 and 6 μm multi-LOCI EHBs show high decoding accuracy, as 28 and 30 clusters from 3 and 6 μm barcodes can be clearly distinguished, respectively (Figure 1b,c). Furthermore, multi-LOCI assays of 3 and 6 μm EHB@ABs were compared using 0 and 1 ng/mL

https://doi.org/10.1021/acsomega.1c06236
ACS Omega 2022, 7, 2344−2355

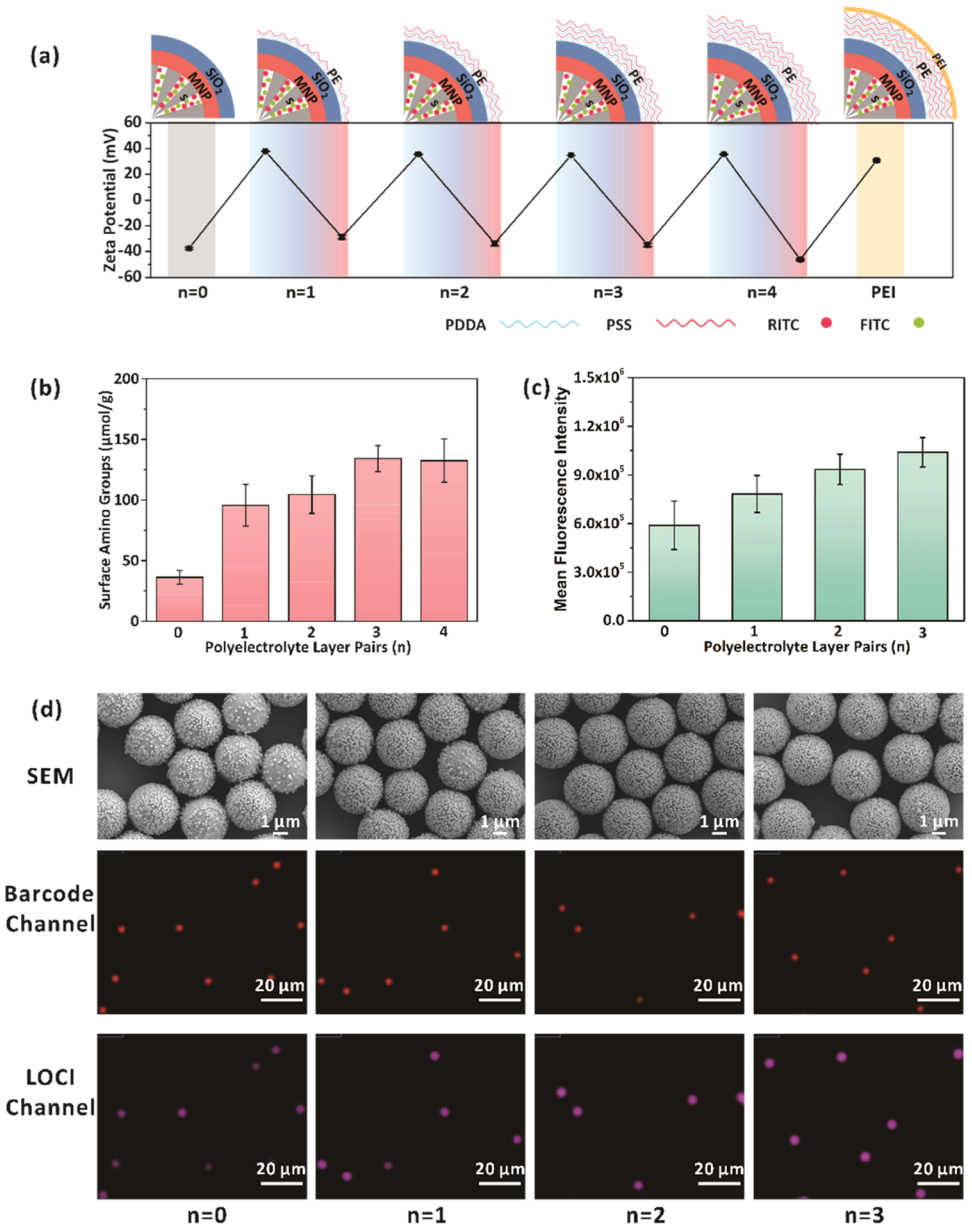

Figure 2. (a) ζ-Potential of 3 μm EHBs continuously modified with four PDDA/PSS pairs and one layer of PEI. (b) Bar plot of densities of surface amino groups on EHB@(PSS/PDDA)*n*@PEI (*n* from 0 to 4) measured using the ITL/DTNB method. (c) Bar plot of fluorescence intensities of EHB@(PSS/PDDA)*n*@PEI@ABs (*n* from 0 to 3) with excitation at 378/52 nm. (d) SEM and fluorescence images of EHB@(PSS/PDDA)*n*@PEI@ABs (*n* from 0 to 3) of barcode F0R1. Fluorescence images illustrate both the barcode channels and the LOCI channel excited at 554/23 and 378/52 nm, respectively.

IFN-γ as analytes under different incubation times. Images were collected and analyzed to obtain barcode and LOCI signal intensities of each EHB@ABs. However, because the surface area of a 6 μm bead is four times larger than that of a 3 μm bead, the pixel numbers of 3 and 6 μm beads in images are different (Figure S1). To make the data of different-sized beads comparable, the mean gray value of all pixels of every EHB@ABs was calculated as its LOCI intensity, and the mean LOCI intensities from all EHB@ABs were plotted in Figure 1d. It is observed that with extended incubation time, both 3 and 6 μm EHB@ABs exhibit a consistent increase in LOCI intensity in the positive detection group, while no increase is observed for EHB@ABs in the control group. Especially, the signal-to-background ratio of 3 μm EHB@ABs is slightly higher than that of 6 μm EHB@ABs at each time point (Figure 1e), possibly because smaller beads have higher reaction kinetics that is derived from fast Brownian motion. Therefore, 3 μm EHBs were employed as the host beads of multi-LOCI barcodes for further investigation.

3.2. Effect of Polyelectrolyte Multilayers on Packing Density of the Host–Guest-Structured Multi-LOCI Barcode. According to the preparation process of host–guest-structured EHBs that our group previously reported, multilayer polyelectrolytes with opposite charges are alternately deposited on the surface of EHBs, to provide binding sites for further assembly of guest ABs.[9,15,22] However, the relationship between the number of adsorbed polyelectrolyte layers and the ABs loading density is yet to be uncovered. Therefore, a number of PSS/PDDA pairs were coated onto the surface of silica-coated EHBs to form EHB@(PSS/PDDA)*n* (*n*

https://doi.org/10.1021/acsomega.1c06236
ACS Omega 2022, 7, 2344−2355

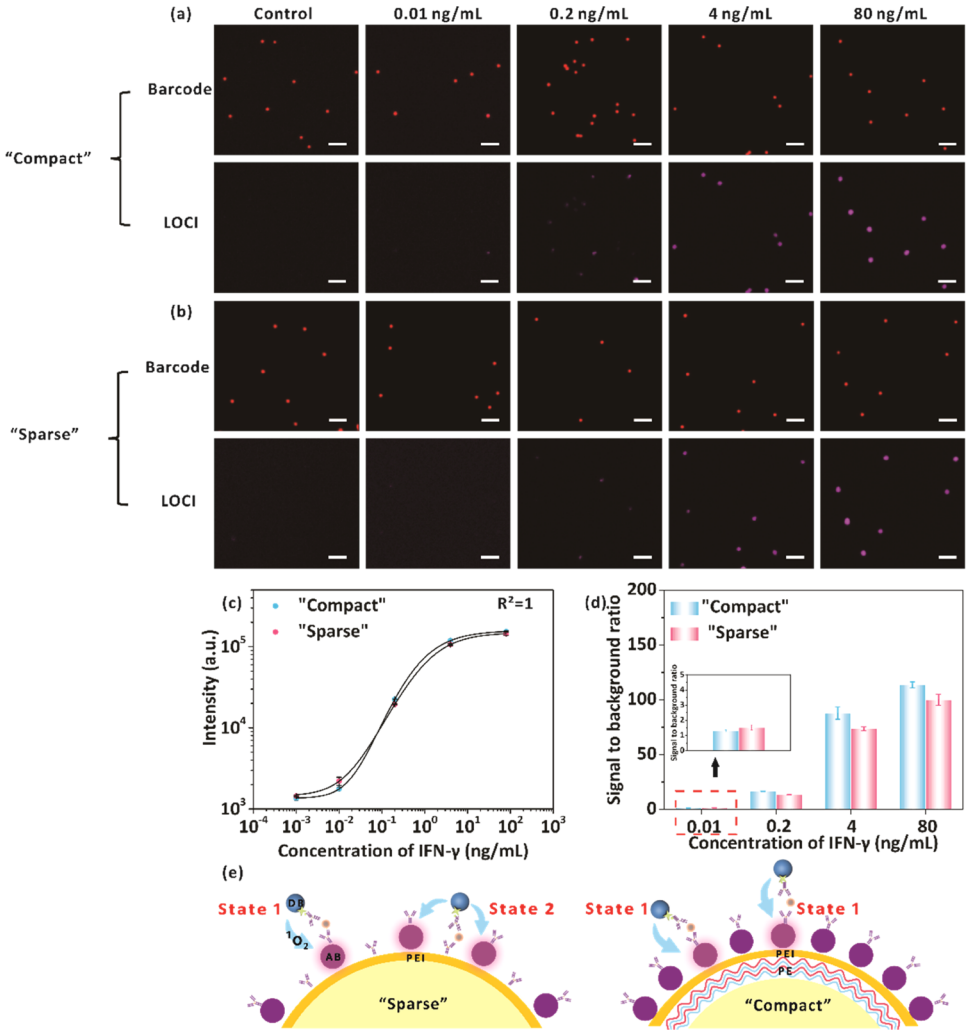

Figure 3. Fluorescence images of EHB@ABs−DB-SA complexes with various concentrations of IFN-γ using (a) "compact" and (b) "sparse" barcodes. Fluorescence images illustrate both the barcode channels and the LOCI channel excited at 554/23 and 680/20 nm, respectively. Scale bar: 20 μm. (c) Calibration curves for IFN-γ quantification using "compact" and "sparse" barcodes, respectively. (d) Bar plot of the corresponding signal-to-background ratios with various concentrations of IFN-γ in (c). (e) Schematic illustration of the two different labels of DB-SA on "sparse" and "compact" barcodes.

ranging from 0 to 4) before carrying out the ABs assembling process. ζ-Potential analysis was performed to verify the multilayered deposition procedure of polyelectrolyte. As depicted in Figure 2a, PDDA with positive charge is deposited on the negatively charged silica surface through electrostatic interactions, resulting in ζ-potential changing from −37 to 38 mV. After the following adsorption of PSS, the ζ-potential returned to a negative value of −29 mV. The subsequent zigzag trend of the ζ-potential values proves that PDDA/PSS pairs are alternatively assembled as expected. Meanwhile, with the increasing number of PDDA/PSS pairs, the surface morphology of EHB@(PSS/PDDA)n in SEM images seems to become smoother and less grainy compared with bare EHBs (Figure S2). These results indicate that a controllable number of polyelectrolyte multilayers are successfully coated onto the surface of EHBs.

Afterward, the prepared EHB@(PSS/PDDA)n were functionalized with PEI, which was confirmed by a change in the ζ-potential value from −46 mv to positive 31 mV (Figure 2a). To clarify whether the deposited PDDA/PSS pairs would affect the abundance of covalent binding sites (primary amino group) provided by PEI, the relationship between the number of PDDA/PSS pairs and the surface primary amino density was further explored. As described in Figure 2b, the amino density of EHBs directly modified with PEI through electrostatic interaction between the hydroxylated silica shell and PEI (EHB@(PSS/PDDA)n @PEI, n = 0) is measured to be 36.2 μmol/g, demonstrating a high density of amino groups on the branched PEI chains. Notably, if one pair of PDDA/PSS is introduced as the interlayer between EHBs and PEI (EHB@(PSS/PDDA)n@PEI, n = 1), the surface amino groups exhibit a remarkable increase in density to 95.6 μmol/g. The possible reason for this is that the multilayered polyelectrolytes provide more binding sites for subsequent PEI adsorption compared with the bare silica surface. The layer-by-layer assembly of polyelectrolytes may form a crisscross branched polymer surface that offers more abundant binding sites for subsequent adsorption of polyelectrolytes with reverse charge, for example, PDDA, PSS, and PEI are alternately adsorbed in turn. In contrast, the number of binding sites (only hydroxyl groups) on the bare silica surface is relatively low. With a further increasing number of PDDA/PSS pairs, the

https://doi.org/10.1021/acsomega.1c06236
ACS Omega 2022, 7, 2344−2355

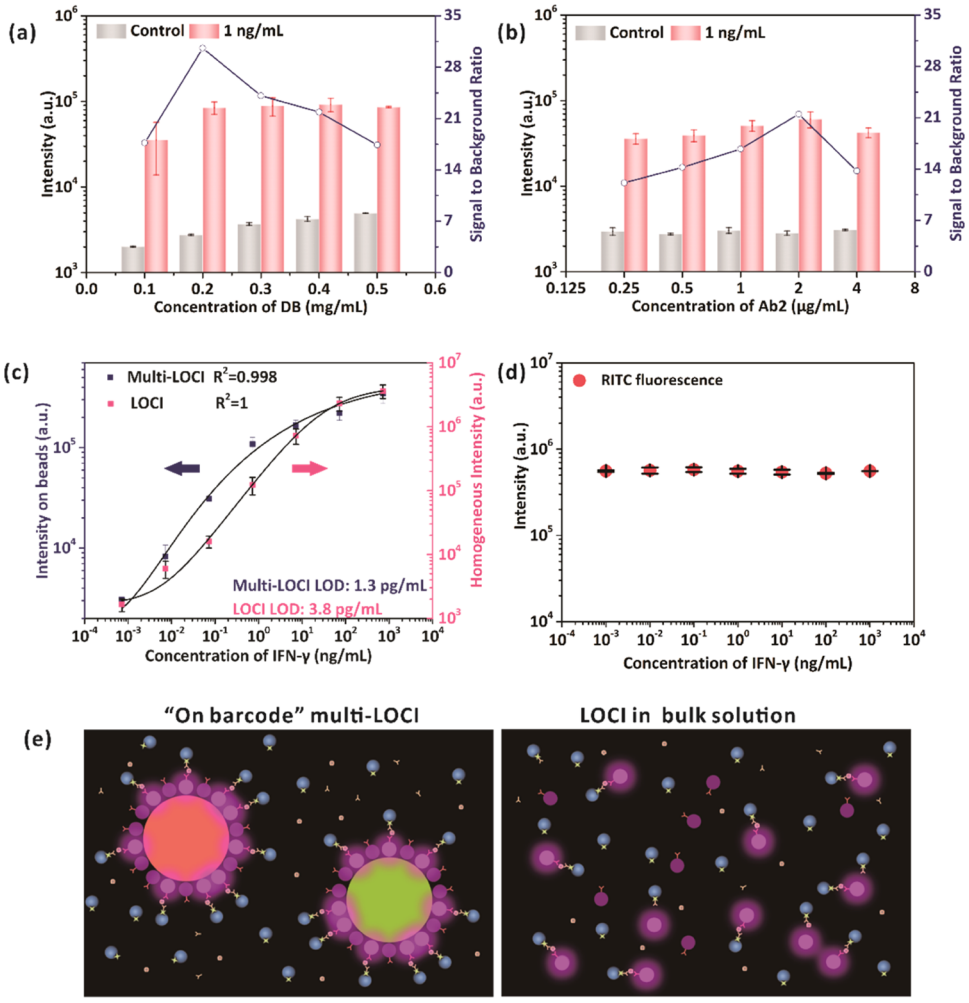

Figure 4. (a) Bar plot of LOCI intensities and the corresponding signal-to-background ratios of 0 and 1 ng/mL IFN-γ with five different DB-SA concentrations (0.1, 0.2, 0.3, 0.4, 0.5 mg/mL). (b) Bar plot of LOCI intensities and the corresponding signal-to-background ratios of 0 and 1 ng/mL IFN-γ with five different biotinylated detection antibody concentrations (0.25, 0.5, 1, 2, 4 μg/mL) (c) Calibration curves for IFN-γ quantification using both LOCI and multi-LOCI methods, respectively. (d) Plots showing the RITC fluorescence intensities of EHB@ABs−DB-SA. (e) Schematic of the "on-barcode" multi-LOCI assay and LOCI signals in the bulk solution.

increase in density slows down and finally reaches a plateau when n = 3. This result is attributed to the assumption that the number of the outer PSS chains tends to be consistent and uniform after consecutive modification of PDDA/PSS pairs, offering a steady surface for PEI deposition.

To explore the effect of the surface amino density on subsequent ABs loading density, EHB@(PSS/PDDA)n@PEI with a different number of PSS/PDDA pairs (n varied from 0 to 3, since the increase of surface amino density reached a plateau when n = 3) was further coated with ABs following a carbodiimide-based coupling approach, as described in the previous study.[22] The SEM images of the fabricated EHB@(PSS/PDDA)n@PEI@ABs are shown in Figure 2d. An increase of the ABs packing density is observed with the increased number of deposited PSS/PDDA pairs, which is also in accord with the increase in surface amino density of microbeads. In addition, the fluorescence images of EHB@(PSS/PDDA)n@PEI@ABs were also measured, where ABs were excited at 378/52 nm (Figure 2c). In agreement with SEM results, the fluorescence signal of ABs exhibits a linear elevation with an increased number of PSS/PDDA pairs, owing to more ABs being assembled on microbeads. Meanwhile, the coefficient of variation (CV) for the fluorescence intensity decreases sharply from 25% to 9% when n ranges from 0 to 3, suggesting that a high ABs packing density results in a more uniformed ABs assembly. These results demonstrate that the ABs packing density of host−guest-structured multi-LOCI barcodes is strongly relevant to the deposition state of polyelectrolytes, owing to the multilayered polyelectrolyte substrate providing rich surface amino groups and a soft landing surface for ABs.[15]

3.3. Detection Performance of Multi-LOCI Barcodes with Different Packing Densities. To study the effect of ABs packing density on detection performance, two types of barcodes with low and high ABs loading densities (EHB@PEI@ABs and EHB@$(PSS/PDDA)_2$@PEI@ABs, referred to as "sparse" and "compact", respectively) were selected as they represent two typical barcodes with a distinct packing density and the simplicity of a practical fabrication process. The multi-LOCI assay performance of the two barcodes was then compared. Fluorescence images in barcode and LOCI channel for IFN-γ quantification were acquired (Figure 3a,b). It can be observed that LOCI signals of either "sparse" or "compact" barcode show a consistent growth with the increase of IFN-γ

https://doi.org/10.1021/acsomega.1c06236
ACS Omega 2022, 7, 2344−2355

concentration, which is attributed to more DB-SA loaded onto the barcodes. Furthermore, the two calibration curves are plotted to compare the detection performance of "sparse" and "compact" barcodes (Figure 3c). LOCI intensities of "compact" barcodes are slightly higher than those of "sparse" barcodes under a high concentration of IFN-γ (0.2, 4, 80 ng/mL). This is possibly ascribed to more available ABs on the surfaces of "compact" barcodes, resulting in higher LOCI intensity when sufficient DB-SA is deposited on ABs via the formation of immunocomplexes. In addition, "compact" barcodes show a slightly higher signal-to-background ratio compared with that of "sparse" barcodes. This is ascribed to more ABs of "compact" barcodes being "turned on" in the presence of analytes, while the background signals for both "compact" and "sparse" are similar in the absence of analytes (Figure 3d). With respect to the overall performance, however, the two barcodes exhibit comparable sensitivity, dynamic range, and precision. This unexpected result that the performance of "sparse" barcodes is comparable with that of "compact" barcodes may be due to the following possible reason illustrated in Figure 3e. For "sparse" barcodes, there are two surface states after immune reaction: (1) DB-SA is bound directly on the surface of guest ABs of multi-LOCI barcode via affinity interaction between SA and biotinylated detection antibody and (2) DB-SA is caught on the exposed barcode surface that is embedded in the middle of two ABs since the barcode surface also has the immobilized capture antibodies. For "compact" barcodes, however, only state 1 exists. Undoubtedly, LOCI signals under state 1 for "compact" barcodes are higher than those for "sparse" barcodes due to more ABs being available. Nevertheless, DBs under state 2 for "sparse" barcodes could also induce luminescence oxygen channeling signal since their distances to ABs are still in close proximity, which acts as an extra pathway to provoke LOCI signals from ABs. Therefore, the "sparse" and "compact" barcodes exhibit similar LOCI intensities. Thanks to the unique tailor-designed structure of ABs being enriched on individual multi-LOCI barcodes, the DB-SA labeling site becomes more diverse and flexible. Hence, it is no longer only dependent on the direct immune reaction between ABs and DB-SA to induce LOCI signals. In contrast, for conventional LOCI where ABs are uniformly dispersed in bulk solution, LOCI signals are provoked only when ABs and DB-SA are directly bonded. This interesting result inspires us to think that the multi-LOCI barcodes are highly flexible and robust, tremendously reducing complexity and elaboration during the fabrication process.

3.4. Optimization of the Multi-LOCI Assay System and Detection Performance Evaluation of Multiplexed Assay. Apart from the barcode structure, the assay system including the power of 680 nm laser diode and the concentrations of DB-SA and detection antibody also plays a decisive role in the final multi-LOCI detection performance. For the multi-LOCI detection system, DB-SA, a key component that generates singlet oxygen, is labeled onto the surface of the barcode mediated by detection antibody via biotin−streptavidin interaction. It is inevitable that the concentration of DB-SA directly affects its labeling process, further influencing the LOCI signal. Herein, the relationship between the amount of DB-SA and the multi-LOCI detection performance was investigated carefully by adjusting DB-SA concentrations ranging from 0.1 to 0.5 mg/mL. As shown in Figure 4a, the LOCI signal of the IFN-γ positive group increases sharply when the concentration of DB-SA increases from 0.1 to 0.2 mg/mL, indicating that more DB-SA loaded onto EHB@ABs can cause more effective production of singlet oxygen. The LOCI signal remains consistent as the concentration of DB-SA varies from 0.2 to 0.5 mg/mL, suggesting a saturated status of DB-SA labeling. However, the background signal also shows consistent growth with an increased amount of DB-SA. Thus, the highest signal-to-background ratio is observed at 0.2 mg/mL of DB-SA, which is chosen as the relatively optimal concentration.

To explore the relationship between the power of 680 nm laser diode and the multi-LOCI performance, we measured the LOCI signal intensity of different concentrations of IL-10 at laser powers of 5, 4, 3.5, 3, 2.5, and 1.9 W, respectively (Figure S3, Supporting Information). It is shown that LOCI intensities increased with enhanced laser power within the whole IL-10 concentration range, demonstrating that more singlet oxygens were generated by DB-SA with higher laser energy. Besides, the background signal also increased with an increase of laser power (Figure S3a, Supporting Information). It should be noted that the signal-to-background ratios also increased with enhanced laser power within the whole IL-10 concentration range (Figure S3b, Supporting Information). Thus, we can conclude that higher laser power results in better assay performance. Since the highest power of the 680 nm laser diode that we used here is 5 W, it is chosen as the optimized laser power for all multi-LOCI experiments.

Moreover, the investigation of an optimized detection antibody concentration is critical because the detection antibody bridges analyte with DB-SA via specific antigen−antibody binding and biotin−streptavidin interaction. A series of experiments were carried out to explore the optimal conditions of detection antibody by comparing the LOCI signal of 1 ng/mL cytokine with that of the control, with the candidate detection antibody concentration varying from 0.25 to 4 μg/mL. Taking IFN-γ as an example, the LOCI signal increases as the concentration of the detection antibody increases from 0.25 μg/mL to 2 μg/mL (Figure 4b). This phenomenon is ascribed to the formation of more immune complexes, providing more biotin sites for the loading of DB-SA. The LOCI signal decreases when the concentration of the detection antibody further increases to 4 μg/mL, suggesting that excess free biotinylated detection antibody in reaction solution competes with the conjugated detection antibody bound onto the surface of barcode, weakening the deposition quantity of DB-SA and further reducing LOCI signals. Meanwhile, the amount of detection antibodies shows no influence on the background signals. Hence, the optimized detection antibody concentration is 2 μg/mL according to its highest signal-to-background ratio. Similar phenomena are observed for detection antibodies corresponding to the other three cytokines. The optimized concentrations of different targets are in the range of 0.25−2 μg/mL (Figure S4a−c, Supporting Information).

After the optimization of the assay system, multi-LOCI performance was demonstrated by quantifying four cytokines with a series of concentrations. As can be seen from the calibration curve for detecting IFN-γ (Figure 4c), the multi-LOCI performance shows a remarkable improvement compared with our previous work with the limit of detection (LOD) decreasing from 55.6 to 1.3 pg/mL.[22] LODs of IL-6, IL-10, and IL-17A are determined to be 3.8, 16.6, and 62.9 pg/mL, respectively, flowing the 3σ criteria. IL-10 and IL-17A also

https://doi.org/10.1021/acsomega.1c06236
ACS Omega 2022, 7, 2344−2355

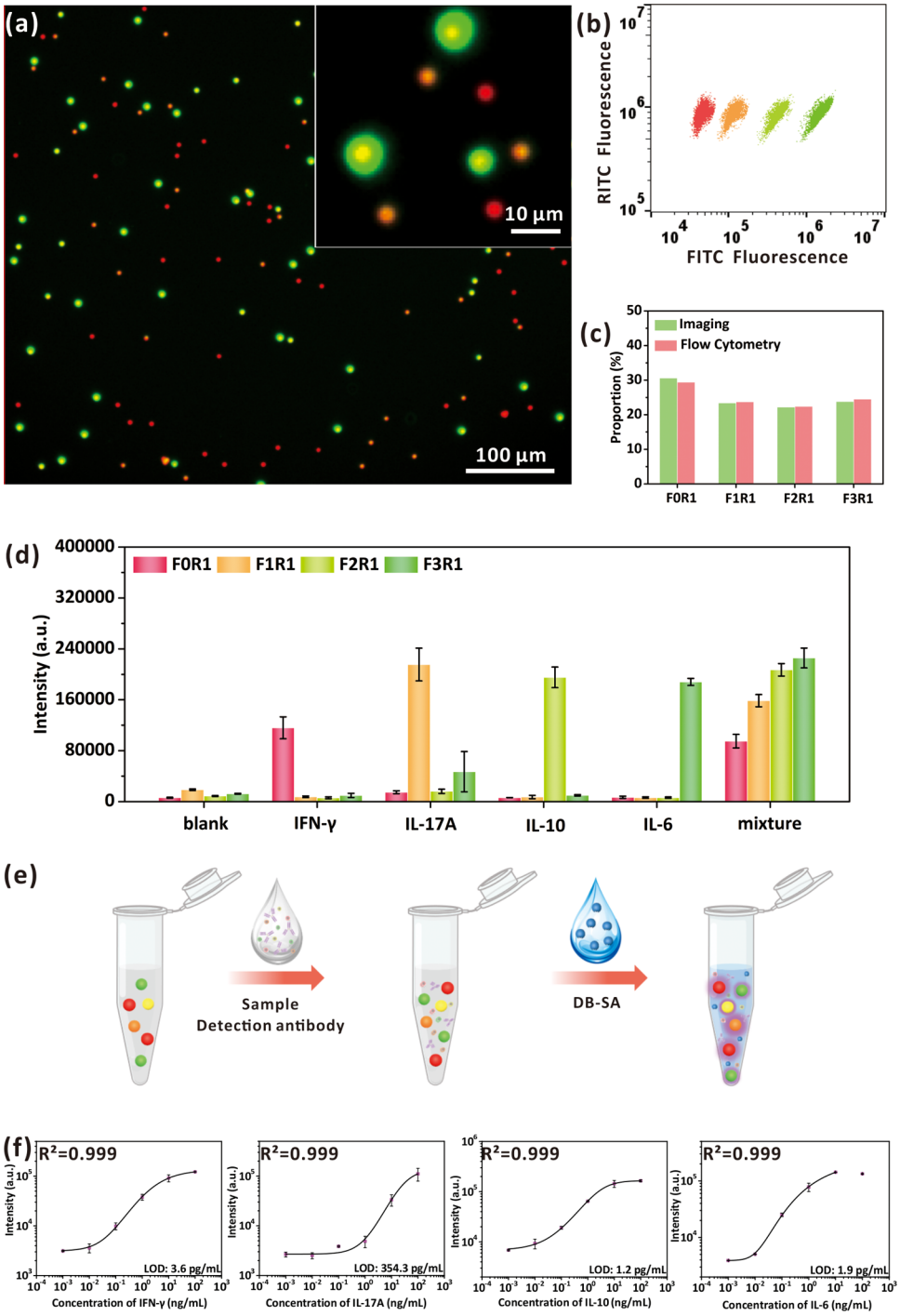

Figure 5. (a) Fluorescence image of four-plexed multi-LOCI EHBs. (b) Scatter plot of the library of the barcodes obtained by the imaging-based decoding. (c) Proportion of each type of barcode obtained by both imaging-based decoding and flow cytometry decoding. (d) Histogram of the mean LOCI intensities of mixed barcodes in the presence of 1 ng/mL IFN-γ, IL-17A, IL-10, and IL-6 and a mixture of the four cytokines as indicated. (e) Scheme of the multi-LOCI "mix-and-measure" protocol for the multiplexed assay. (f) Calibration curves for multiplexed detection of IFN-γ, IL-17A, IL-10, and IL-6 using the multi-LOCI approach, respectively.

demonstrated higher sensitivity than our previous work (LOD of IL-10 is 43.1 pg/mL and LOD of IL-17A is 91.6 pg/mL) (Figure S4d–f).[22] Moreover, the barcode signals remain stable with the CVs of intensities as low as 3.2% regardless of the varied analyte concentrations, which ensures the decoding accuracy (Figure 4d). Besides, the assay performance of multi-LOCI using IFN-γ as a model is further compared with the conventional LOCI approach, which is well-known as a homogeneous assay with high sensitivity. As shown in Figure 4d, multi-LOCI exhibits even higher sensitivity than the classical LOCI (LOD to be 3.8 pg/mL). This result surprised us because theoretically, LOCI has higher reaction kinetics since 200 nm sized ABs and DB-SA are homogeneously dispersed in solution, compared with multi-LOCI whose barcode size is in the micron scale. The reasons for this unexpected high sensitivity are speculated as follows. First,

https://doi.org/10.1021/acsomega.1c06236
ACS Omega 2022, 7, 2344−2355

with respect to signal acquisition for conventional LOCI, overall signals from the bulk solution that contains both cross-linked ABs-DB-SA complexes that generate LOCI signals and large amounts of free ABs and DB-SA particles that generate background signals are simultaneously collected. Thus, the LOCI signal is more susceptible to the background signal. In contrast, for on-barcode multi-LOCI, *in situ* LOCI signals from individual barcodes are collected via the imaging approach, significantly reducing the interference of background noises from the bulk solution. Second, LOCI signals localized on individual barcodes are more concentrated for on-barcode multi-LOCI assay, compared with conventional LOCI whose signals are diluted in the bulk solution (Figure 4e). Thanks to the unique on-barcode assay format where the LOCI process is conducted *in situ* on individual barcodes, we suppose that multi-LOCI assay could overcome the shortage of relatively lower reaction kinetics and achieve even better sensitivity than conventional LOCI.

More importantly, the multi-LOCI platform not only provides a rapid and simple quantification method but also realizes high throughput and multiplexed assays in one reaction. As a proof of concept, four types of barcodes, denoted as F0R1, F1R1, F2R1, and F3R1 (obtained by adjusting the ratio of FITC and RITC), were assigned to detect IFN-γ, IL-17A, IL-10, and IL-6, respectively. The capacity of decoding based on imaging was verified for the multi-LOCI platform. After automation and high throughput image analysis, four clusters are clearly distinguished without overlaps (Figure 5b). Moreover, the proportion of each type of barcode gained by imaging was 30.6, 23.4, 22.2, and 23.8%, which is in accordance with that acquired by flow cytometry (Figure 5c, 29.4, 23.7, 22.4, 24.5%, respectively). These results demonstrate that the imaging-based decoding strategy has high accuracy and throughput in multiplexed assays.

To evaluate the specificity of the multi-LOCI platform for multiplexed assay, six groups of experiments were carried out (blank group: no cytokine was added; IFN-γ, IL-17A, IL-10, and IL-6 groups: each of the four cytokines added separately; mixture: all four cytokines were simultaneously added). It was found out that the LOCI signal in a specific barcode significantly increased only when its corresponding cytokine was added (Figure 5d), and for the blank group, no LOCI signal was observed for each barcode, illustrating high specificity for the multi-LOCI platform.

Moreover, calibration curves for multiplexed detection were established using samples containing a mixture of the four cytokines in different concentrations (Figure 5e). As shown in Figure 5f, in accordance with the performance of the single-plexed assay, higher sensitivity of the multiplexed assay is observed than our previous work after comprehensive optimization of the assay system developed in this work, and the LODs of IFN-γ, IL-17A, IL-10, and IL-6 are calculated to be 3.6, 354.3, 1.2, and 1.9 pg/mL, respectively. The phenomenon of the sensitivity of IL-17A for multiplexed detection being lower than that of the single-plexed assay may due to the competition response between IL-17A with the other three cytokines. Importantly, detection of these multiple analytes was accomplished within one reaction without the need for washing steps, which remarkably reduces requirements of sample volume and improves detection throughput, demonstrating a facile biodetection platform combining both high multiplexing and sensitivity.

4. CONCLUSIONS

In summary, through a deeper investigation on the structure−performance relationship of multi-LOCI barcodes, this work found out that the number of surface amino groups that originated from PEI showed significant growth if polyelectrolyte pairs were employed, resulting in a uniform and high-density assembly of ABs onto the EHBs. Interestingly, the detection performance of multi-LOCI between the "sparse" and "compact" barcodes was neck and neck. Besides, it was worth noting that multi-LOCI exhibited comparable sensitivity with the classical LOCI after comprehensive optimization of the assay system. These unexpected results benefitted from the ingenious structural design of the multi-LOCI barcode, making this novel "on-barcode" multi-LOCI platform highly flexible and robust. It is believed that with the advantages of high multiplexing and a facile "mix-and-measure" protocol, together with the aid of portable microfluidics or devices, the multi-LOCI platform will open new pathways toward robust, highly sensitive, and multiplexed point-of-care diagnostics.

■ ASSOCIATED CONTENT

Supporting Information

The Supporting Information is available free of charge at https://pubs.acs.org/doi/10.1021/acsomega.1c06236.

Three-dimensional (3D) mesh diagrams originating from a single 3 and 6 μm barcode in fluorescence images (Figure S1); SEM images of EHBs (Figure S2); and optimization results of 680 nm laser power and detection antibody concentration (Figures S3 and S4) (PDF)

■ AUTHOR INFORMATION

Corresponding Authors

Qingsheng Guo − *School of Biomedical Engineering, Shanghai Jiao Tong University, Shanghai 200030, P. R. China*; Email: shockwow@sjtu.edu.cn

Hong Xu − *School of Biomedical Engineering, Shanghai Jiao Tong University, Shanghai 200030, P. R. China*; orcid.org/0000-0002-2787-5806; Email: xuhong@sjtu.edu.cn

Authors

Zuying Feng − *School of Biomedical Engineering, Shanghai Jiao Tong University, Shanghai 200030, P. R. China*; orcid.org/0000-0002-9236-3030

Yao Wang − *School of Biomedical Engineering, Shanghai Jiao Tong University, Shanghai 200030, P. R. China*; orcid.org/0000-0003-0470-9511

Yunfei Ge − *School of Biomedical Engineering, Shanghai Jiao Tong University, Shanghai 200030, P. R. China*

Zhiying Zhang − *School of Biomedical Engineering, Shanghai Jiao Tong University, Shanghai 200030, P. R. China*

Yan Wu − *School of Biomedical Engineering, Shanghai Jiao Tong University, Shanghai 200030, P. R. China*

Qilong Li − *School of Biomedical Engineering, Shanghai Jiao Tong University, Shanghai 200030, P. R. China*

Hajar Masoomi − *School of Biomedical Engineering, Shanghai Jiao Tong University, Shanghai 200030, P. R. China; School of Integrated Technology, Gwangju Institute of Science and Technology, Gwangju 61005, South Korea*; orcid.org/0000-0002-5776-6141

https://doi.org/10.1021/acsomega.1c06236
ACS Omega 2022, 7, 2344−2355

Hongchen Gu − *School of Biomedical Engineering, Shanghai Jiao Tong University, Shanghai 200030, P. R. China*

Complete contact information is available at: https://pubs.acs.org/10.1021/acsomega.1c06236

Author Contributions

The manuscript was written through the contributions of all authors. All authors have given approval to the final version of the manuscript.

Notes

The authors declare no competing financial interest.

■ ACKNOWLEDGMENTS

The project was supported by the China Postdoctoral Science Foundation (BR0820016), the National Natural Science Foundation of China (Grant Nos. 21874091, 31927803, and 32101158), and the Innovation Research Plan supported by the Shanghai Municipal Education Commission (Grant No. ZXWF082101). The authors acknowledge the Instrumental Analysis Center of Shanghai Jiao Tong University for the characterization of materials.

■ REFERENCES

(1) Silva, J. M.; Marran, K.; Parker, J. S.; Silva, J.; Golding, M.; Schlabach, M. R.; Elledge, S. J.; Hannon, G. J.; Chang, K. Profiling Essential Genes in Human Mammary Cells by Multiplex RNAi Screening. *Science* **2008**, *319*, 617−620.

(2) Plesa, C.; Sidore, A. M.; Lubock, N. B.; Zhang, D.; Kosuri, S. Multiplexed gene synthesis in emulsions for exploring protein functional landscapes. *Science* **2018**, *359*, 343−347.

(3) Kyriazi, M.-E.; Giust, D.; El-Sagheer, A. H.; Lackie, P. M.; Muskens, O. L.; Brown, T.; Kanaras, A. G. Multiplexed mRNA Sensing and Combinatorial-Targeted Drug Delivery Using DNA-Gold Nanoparticle Dimers. *ACS Nano* **2018**, *12*, 3333−3340.

(4) Yin, Z.; Ramshani, Z.; Waggoner, J. J.; Pinsky, B. A.; Senapati, S.; Chang, H.-C. A non-optical multiplexed PCR diagnostic platform for serotype-specific detection of dengue virus. *Sens. Actuators, B* **2020**, *310*, No. 127854.

(5) Orlov, A. V.; Pushkarev, A. V.; Znoyko, S. L.; Novichikhin, D. O.; Bragina, V. A.; Gorshkov, B. G.; Nikitin, P. I. Multiplex label-free biosensor for detection of autoantibodies in human serum: Tool for new kinetics-based diagnostics of autoimmune diseases. *Biosens. Bioelectron.* **2020**, *159*, No. 112187.

(6) Aynaud, M.-M.; Hernandez, J. J.; Barutcu, S.; Braunschweig, U.; Chan, K.; Pearson, J. D.; Trcka, D.; Prosser, S. L.; Kim, J.; Barrios-Rodiles, M.; Jen, M.; Song, S.; Shen, J.; Bruce, C.; Hazlett, B.; Poutanen, S.; Attisano, L.; Bremner, R.; Blencowe, B. J.; Mazzulli, T.; Han, H.; Pelletier, L.; Wrana, J. L. A multiplexed, next generation sequencing platform for high-throughput detection of SARS-CoV-2. *Nat. Commun.* **2021**, *12*, No. 1405.

(7) Xu, Y.; Wang, H.; Chen, B.; Liu, H.; Zhao, Y. Emerging barcode particles for multiplex bioassays. *Sci. China Mater.* **2019**, *62*, 289−324.

(8) Huang, C.; Wang, Y.; Li, X.; Ren, L.; Zhao, J.; Hu, Y.; Zhang, L.; Fan, G.; Xu, J.; Gu, X.; Cheng, Z.; Yu, T.; Xia, J.; Wei, Y.; Wu, W.; Xie, X.; Yin, W.; Li, H.; Liu, M.; Xiao, Y.; Gao, H.; Guo, L.; Xie, J.; Wang, G.; Jiang, R.; Gao, Z.; Jin, Q.; Wang, J.; Cao, B. Clinical features of patients infected with 2019 novel coronavirus in Wuhan, China. *Lancet* **2020**, *395*, 497−506.

(9) Zhang, D. S.-z.; Jiang, Y.; Yang, H.; Zhu, Y.; Zhang, S.; Zhu, Y.; Wei, D.; Lin, Y.; Wang, P.; Fu, Q.; Xu, H.; Gu, H. Dual-Encoded Microbeads through a Host-Guest Structure: Enormous, Flexible, and Accurate Barcodes for Multiplexed Assays. *Adv. Funct. Mater.* **2016**, *26*, 6146−6157.

(10) Gu, Z.; Zhao, S.; Xu, G.; Chen, C.; Wang, Y.; Gu, H.; Sun, Y.; Xu, H. Solid-phase PCR based on thermostable, encoded magnetic microspheres for simple, highly sensitive and multiplexed nucleic acid detection. *Sens. Actuators, B* **2019**, *298*, No. 126953.

(11) Joos, T. O.; Stoll, D.; Templin, M. F. Miniaturised multiplexed immunoassays. *Curr. Opin. Chem. Biol.* **2002**, *6*, 76−80.

(12) Houser, B. Bio-Rad's Bio-Plex suspension array system, xMAP technology overview. *Arch. Physiol. Biochem.* **2012**, *118*, 192−196.

(13) Lim, C. T.; Zhang, Y. Bead-based microfluidic immunoassays: the next generation. *Biosens. Bioelectron.* **2007**, *22*, 1197−1204.

(14) Wang, Y.; Chen, C.; He, J.; Cao, Y.; Fang, X.; Chi, X.; Yi, J.; Wu, J.; Guo, Q.; Masoomi, H.; Wu, C.; Ye, J.; Gu, H.; Xu, H. Precisely Encoded Barcodes through the Structure-Fluorescence Combinational Strategy: A Flexible, Robust, and Versatile Multiplexed Biodetection Platform with Ultrahigh Encoding Capacities. *Small* **2021**, *17*, No. 2100315.

(15) Lu, S.; Zhang, D. S.; Wei, D.; Lin, Y.; Zhang, S.; He, H.; Wei, X.; Gu, H.; Xu, H. Three-Dimensional Barcodes with Ultrahigh Encoding Capacities: A Flexible, Accurate, and Reproducible Encoding Strategy for Suspension Arrays. *Chem. Mater* **2017**, *29*, 10398−10408.

(16) Wu, W.; Yu, X.; Gao, M.; Gull, S.; Shen, L.; Wang, W.; Li, L.; Yin, Y.; Li, W. Precisely Encoded Barcodes Using Tetrapod CdSe/CdS Quantum Dots with a Large Stokes Shift for Multiplexed Detection. *Adv. Funct. Mater.* **2020**, *30*, No. 1906707.

(17) Lin, G.; Baker, M. A. B.; Hong, M.; Jin, D. The Quest for Optical Multiplexing in Bio-discoveries. *Chem* **2018**, *4*, 997−1021.

(18) Wei, X.; Bian, F.; Cai, X.; Wang, Y.; Cai, L.; Yang, J.; Zhu, Y.; Zhao, Y. Multiplexed Detection Strategy for Bladder Cancer MicroRNAs Based on Photonic Crystal Barcodes. *Anal. Chem.* **2020**, *92*, 6121−6127.

(19) Bian, F.; Sun, L.; Cai, L.; Wang, Y.; Zhao, Y.; Wang, S.; Zhou, M. Molybdenum disulfide-integrated photonic barcodes for tumor markers screening. *Biosens. Bioelectron* **2019**, *133*, 199−204.

(20) Akama, K.; Shirai, K.; Suzuki, S. Highly sensitive multiplex protein detection by droplet-free digital ELISA. *Electron. Commun. Japan* **2019**, *102*, 43−47.

(21) Wang, C.; Zhan, R.; Pu, K.-Y.; Liu, B. Cationic Polyelectrolyte Amplified Bead Array for DNA Detection with Zeptomole Sensitivity and Single Nucleotide Polymorphism Selectivity. *Adv. Funct. Mater.* **2010**, *20*, 2597−2604.

(22) Guo, Q.; Wang, Y.; Chen, C.; Wei, D.; Fu, J.; Xu, H.; Gu, H. Multiplexed Luminescence Oxygen Channeling Immunoassay Based on Dual-Functional Barcodes with a Host−Guest Structure: A Facile and Robust Suspension Array Platform. *Small* **2020**, *16*, No. 1907521.

(23) Ullman, E. F.; Kirakossian, H.; Singh, S.; Wu, Z. P.; Irvin, B. R.; Pease, J. S.; Switchenko, A. C.; Irvine, J. D.; Dafforn, A.; Skold, C. N. Luminescent oxygen channeling immunoassay: measurement of particle binding kinetics by chemiluminescence. *Proc. Natl. Acad. Sci. U.S.A.* **1994**, *91*, 5426−5430.

(24) Ullman, E. F.; Kirakossian, H.; Switchenko, A. C.; Ishkanian, J.; Ericson, M.; Wartchow, C. A.; Pirio, M.; Pease, J.; Irvin, B. R.; Singh, S.; Singh, R.; Patel, R.; Dafforn, A.; Davalian, D.; Skold, C.; Kurn, N.; Wagner, D. B. Luminescent oxygen channeling assay (LOCI): sensitive, broadly applicable homogeneous immunoassay method. *Clin. Chem.* **1996**, *42*, 1518−1526.

(25) Masoomi, H.; Wang, Y.; Chen, C.; Zhang, J.; Ge, Y.; Guo, Q.; Gu, H.; Xu, H. A facile polymer mediated dye incorporation method for fluorescence encoded microbeads with large encoding capacities. *Chem. Commun.* **2021**, *57*, 4548−4551.

(26) Zhang, X.; Su, Z. Polyelectrolyte-multilayer-supported Au@Ag core-shell nanoparticles with high catalytic activity. *Adv. Mater* **2012**, *24*, 4574−4577.

(27) Ngo, T. T. Colorimetric determination of reactive amino groups of a solid support using Traut's and Ellman's reagents. *Appl. Biochem. Biotechnol.* **1986**, *13*, 213−219.

(28) Tyllianakis, P. E.; Kakabakos, S. E.; Evangelatos, G. P.; Ithakissios, D. S. Colorimetric determination of reactive primary amino groups of macro- and microsolid supports. *Appl. Biochem. Biotechnol.* **1993**, *38*, 15−25.

(29) Qu, Z.; Xu, H.; Ning, P.; Gu, H. A facile, one-step method for the determination of accessible surface primary amino groups on solid carriers. *Surf. Interface Anal.* **2012**, *44*, 1309−1313.
(30) Leng, Y.; Sun, K.; Chen, X.; Li, W. Suspension arrays based on nanoparticle-encoded microspheres for high-throughput multiplexed detection. *Chem. Soc. Rev.* **2015**, *44*, 5552−5595.
(31) Wilson, R.; Cossins, A. R.; Spiller, D. G. Encoded microcarriers for high-throughput multiplexed detection. *Angew. Chem., Int. Ed.* **2006**, *45*, 6104−6117.

https://doi.org/10.1021/acsomega.1c06236
ACS Omega 2022, 7, 2344−2355